

Article

Numerical Simulation and Temperature Modeling of Magnesium Alloy Strip Rolled by Heated Roll

Ruibin Mei ^{1,2,*} , Lihao Chen ², Li Bao ², Changsheng Li ¹ and Xianghua Liu ¹

¹ State Key Laboratory of Rolling and Automation, Northeastern University, Shenyang 110819, China; lixs@mail.neu.edu.cn (C.L.); liuxh@mail.neu.edu.cn (X.L.)

² School of Resources and Materials, Northeastern University at Qinhuangdao, Qinhuangdao 066004, China; 2272366@stu.neu.edu.cn (L.C.); baoli@neuq.edu.cn (L.B.)

* Correspondence: meiruibin@neuq.edu.cn

Abstract: A prediction model for the outlet temperature of magnesium alloy strips in the process of heated-roll rolling was established by using linear fitting and nonlinear regression methods. By inputting the rolling parameters into the model, the outlet temperature of the strip can be accurately predicted, which will then optimize and regulate the properties and microstructures of the magnesium alloys in the rolled form. To verify the reliability of the model, heat transfer experiments of the magnesium alloy rolled by heated rolls were carried out. The results show that under the same conditions, the actual outlet temperature measured experimentally matches well with the outlet temperature predicted by the model, and the relative error is kept within 10%. In the modeling process, Deform V11.0 software was used to simulate the thermal–mechanical behavior of the magnesium alloy rolled by the heated roll. In the process of analyzing the simulated heat transfer, it was found that the temperature rise of the surface and the core is divided into three identical stages: the slow rise, the fast rise, and the thermal equilibrium stages. In addition, the mechanical behavior of the rolling deformation zone was also analyzed, and the strip was subjected to direct heat transfer from the heated rolls during the hot rolling process so that the softening played a major role and the stress value gradually decreased from the middle of the deformation zone to the inlet end and the outlet end. This is so that it can be known that the process of being rolled by the heated rolls not only improves the rolling efficiency, but also ensures the deformation temperature and obtains fine grains.

Keywords: heated rolls; magnesium alloy strip; temperature predictive modeling; numerical simulation



Citation: Mei, R.; Chen, L.; Bao, L.; Li, C.; Liu, X. Numerical Simulation and Temperature Modeling of

Magnesium Alloy Strip Rolled by Heated Roll. *Metals* **2023**, *13*, 1785.

<https://doi.org/10.3390/met13101785>

Academic Editor: Frank Czerwinski

Received: 11 September 2023

Revised: 25 September 2023

Accepted: 17 October 2023

Published: 21 October 2023



Copyright: © 2023 by the authors. Licensee MDPI, Basel, Switzerland. This article is an open access article distributed under the terms and conditions of the Creative Commons Attribution (CC BY) license (<https://creativecommons.org/licenses/by/4.0/>).

1. Introduction

As the lightest metal structural materials, magnesium and its alloys have low density, a high specific strength, a high specific modulus, and high thermal conductivity and are widely used in the fields of electronics, transportation, aerospace, and biomedicine [1–3]. Magnesium alloys have fewer open slip systems at room temperature due to their hexagonal close-packed structure [4–6], which greatly limits their plastic deformation. As an important metal-forming technology, hot rolling is a key technology in the production of magnesium alloy strips because high temperature ensures large deformation, grain refinement, and formability [7–9]. However, due to the contact with the rolls, a large amount of heat loss on the surface leads to a rapid drop in strip temperature and severe work-hardening, and in particular, the thinner the strip, the more pronounced the drop in temperature, which greatly affects the control of microstructure and properties in the rolling process, and the subsequent rolling process [9–11]. To ensure the deformation temperature during multi-pass rolling, intermediate heating is usually used as an important factor in regulating rolling efficiency, strength, and microstructure [12–14].

Although the deformation temperature was ensured by intermediate annealing, which resulted in a significant improvement in plastic deformation, the rolling efficiency and grain

refinement were also significantly reduced and clearly limited [15,16]. Fisher [17] firstly proposed a rolling method using a preheated roll, in which thin strips were rolled with resistance-heated rolls, and the temperature drop rate of the strips during the rolling process was greatly reduced. Mei et al. [18] investigated the thermal deformation behavior of the AZ91 magnesium alloy in different hot-rolled strip with heated rolls (HSR-HR), normal strip rolled with heated rolls (NSR-HR), and normal strip rolled with normal rolls (HSR-NR) processes using the finite element method (FEM), and found that plastic deformation and annealing were achieved synchronously through the heat transfer from the roll surface to the strip during the rolling using a heated roll, which resulted in a significant improvement in the deformability and uniformity of the strip.

Deformation and temperature have important effects on the microstructure and properties of hot-rolled magnesium alloy strips. Specifically, the temperature in the deformation zone is one of the most important parameters in the heated-roll rolling process [19–21]. Therefore, by changing the process parameters to achieve control over the rolling outlet temperature, the purpose of predicting the microstructure and properties of the strip can be achieved [19–21]. A large number of scholars have established an outlet temperature prediction model through simulations and experiments to achieve outlet temperature control, which is of great significance for obtaining magnesium alloy strips with good mechanical properties and microstructure [22–25]. To achieve temperature control, Yu et al. [26] studied the warm rolling process of the AZ31 alloy using thermal–mechanical finite element simulation, analyzed the effects of process parameters on the temperature field and the average temperature of magnesium alloy plates, and established a temperature prediction model. However, no experimental work was performed to validate the simulation results, and the constant normalization method used for modeling increased the prediction error. Sun et al. [27] developed a polynomial mathematical model combining the finite element method (FEM) and experimental data to predict the outlet temperature of the heated-roll warm rolling process for AZ31 plates, but the actual effect of the process parameters on the temperature was not described in the final prediction model. In addition, as a key parameter, the fixed thermal transfer coefficient between the strip and the work roll used in Reference [28] does not accurately describe the contact heat transfer efficiency.

Therefore, based on the relationship between thermal transfer coefficient and rolling pressure, this study focuses on the plastic deformation of normal-temperature AZ91 alloy strips in heated-roll rolling and the effect of rolling parameters on the outlet temperature using the FEM. In addition, a new function is proposed to describe the relationship among outlet temperature, initial thickness, rolling temperature, reduction, and rolling speed. Finally, a comparative study on the ability of the proposed models to predict temperatures was carried out based on experimental data by evaluating their efficiency and accuracy. This work is not only of great significance for the study, control, and optimization of magnesium alloy rolling parameters in the NSR-HR process but also provides a new method to establish a temperature prediction model for rolling parameters.

2. Materials and Methods

2.1. Finite Element Model

As a large deformation process with negligible elastic deformation, rolling is often analyzed by numerical simulation using rigid-plastic finite elements. In this paper, the penalty function method is mainly used to solve the velocity field and stress field. According to the variation principle, the actual velocity field is obtained by minimizing function (1) [29–31].

$$\pi = \int_V \bar{\sigma} \dot{\varepsilon} dV + \frac{K}{2} \int_V (\dot{\varepsilon}_v)^2 dV - \int_{S_F} F_i u_i dS \quad (1)$$

$\bar{\sigma}$ is the equivalent force (MPa), $\dot{\varepsilon}$ is the equivalent strain rate (mm/min), and K is the penalty constant.

The basic task of rigid-plastic finite element analysis is not only to analyze the velocity field and stress field, but also to consider the temperature and deformation of the workpiece

in the molding process and carry out the thermal–mechanical coupling of the temperature field and the velocity field to provide guidance for the optimization of the temperature control and deformation system in the molding process. Plastic deformation is a nonlinear thermal transient process. The variables $T(x, y, z)$ of the transient temperature field should satisfy the three-dimensional differential equation for the thermal conductivity as shown in Equation (2).

$$\rho_m c \frac{\partial T}{\partial t} - \frac{\partial}{\partial x} \left(k_x \frac{\partial T}{\partial x} \right) - \frac{\partial}{\partial y} \left(k_y \frac{\partial T}{\partial y} \right) - \frac{\partial}{\partial z} \left(k_z \frac{\partial T}{\partial z} \right) - \dot{q} = 0 \quad (2)$$

T is the transient temperature of an infinitesimal object (K), ρ_m is the density of the material (kg/m^3), c is the specific heat capacity $\text{J}/(\text{kg} \cdot \text{K})$, t is the time, \dot{q} is the density of the storage heaters (W/kg), and k_x, k_y, k_z are the x, y, z conductivities of the material, respectively.

During hot rolling, the temperature is also affected by deformation and friction work, and the heat generated by plastic deformation and friction can be expressed as follows:

$$\dot{q}_{def} = \eta \bar{\sigma} \dot{\bar{\epsilon}}, \dot{q}_{fric} = \tau |\Delta v| \quad (3)$$

\dot{q}_{def} (W/m^3) and \dot{q}_{fric} (W/m^3) are the heat generation rates in the rolling process for plastic deformation and friction, respectively. η is the coefficient that determines the fraction of deformation energy that is converted to heat. $\bar{\sigma}$ and $\dot{\bar{\epsilon}}$ represent the flow stress and strain rate of the material in a rolling pass, respectively. τ is the frictional shear stress. Δv is the relative slip velocity.

For this paper, finite element simulations were performed by using the commercial software Deform, and the temperature field was analyzed by first determining the heat transfer model. Heat transfer processes during the hot rolling of magnesium alloy strips include contact heat transfer between the work rolls and the strip, natural convection, and thermal radiation [16]. There are different heat transfer models for the air cooling process and the rolling process. Thermal radiation and natural convection are mainly considered in the air cooling process, and the surface emissivity and convective heat coefficients used for the simulation are 0.07 and $11 \text{ W}/(\text{m}^2 \cdot \text{K})$, respectively. The contact heat transfer between the working rolls and the strip leads to the main heat loss in the hot rolling process, and the relationship between the HTC (the thermal resistance heat transfer coefficient) produced by the strip and the rolls and the Pm (the roll pressure) during the hot rolling process was obtained by DING [32].

The heat transfer coefficient for each stage can be expressed as follows:

$$H_{TC} = 0.1133 \times P_m + 28.92476 \quad (4)$$

The properties of AZ91 alloy vary with temperature, but these property parameters are often assumed to be constants in analyzing mechanical–thermal coupling problems. They are as follows: density of $1820 \text{ kg}/\text{m}^3$, modulus of elasticity of 44.8 MPa , Poisson's ratio of 0.35, coefficient of thermal expansion of $2.6 \times 10^{-5} \text{ K}^{-1}$, electrical conductivity of $72 \text{ W}/\text{m} \cdot \text{K}$, specific heat capacity of $1.9 \text{ kJ}/\text{kg} \cdot \text{K}$, and coefficient of friction of 0.3. Constitutive equations of AZ91 magnesium alloys used to solve the deformation process for different strain rates and temperatures are given in Reference [33].

Specific parameters for preprocessing during Deform analysis are shown below. The roll diameter used for numerical simulation analysis is 300 mm; the strip length is 500 mm; the inlet thicknesses are set to 4, 8, 12, and 16 mm with reductions of 10%, 20%, 30%, and 40%; and the rolling speeds are 0.01 m/s, 0.05 m/s, 0.1 m/s, and 0.5 m/s. The temperature settings for various heating and rolling processes were as follows: Under the NSR-HR condition, the roll surface temperatures were $200 \text{ }^\circ\text{C}$, $250 \text{ }^\circ\text{C}$, $300 \text{ }^\circ\text{C}$, $350 \text{ }^\circ\text{C}$, and $400 \text{ }^\circ\text{C}$, and the strip inlet temperature was set to $20 \text{ }^\circ\text{C}$. The strip was divided into 100 elements in the rolling direction and 4 elements in the thickness direction, totaling 400 elements,

and the rolls were divided into 1000 elements using a quadrilateral mesh to improve the calculation accuracy. Using the meshing method, the interference size was set to 0.1 mm to prevent mesh deformation which might lead to convergence of the calculation. Figure 1 depicts the established finite element model.

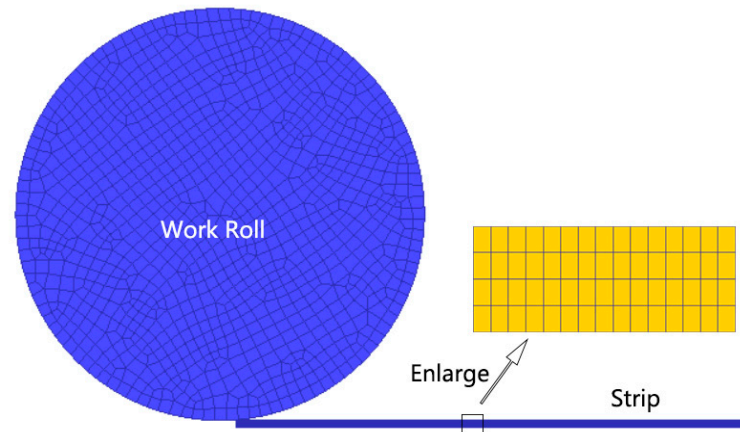


Figure 1. Finite element mesh.

2.2. Test Methods for Hot Rolling

Commercial AZ91 magnesium alloy plates with a chemical composition of 8.87 wt% aluminum, 0.95 wt% zinc, 0.13 wt% manganese, 0.02 wt% silicon, and the remainder magnesium were used as rolled test materials. The plates were initially 2, 4, 6, and 8 mm thick and then wire-cut into 100 mm × 60 mm specimens. The specimens were heated to 400 °C in a resistance furnace, homogenized, and annealed for 5 h. After homogenization, the samples were cleaned and prepared for use. In the hot rolling test, the surface temperature of the rolls was heated to 200, 250, 300, and 350 °C by induction coils. The total reduction was controlled at about 20, 40, and 60%; no annealing treatment was carried out between passes; the specimens were cooled at room temperature after rolling; and the rolling speeds were set at 0.01, 0.05, and 0.1 m/s.

3. Results and Discussion

3.1. Temperature Analysis

Since the simplified model of the rolling process is a symmetric structure, the geometric modeling process only requires the creation of the symmetric half of the strip about the x -axis and an upper roll; the part maintains the same coefficients of temperature and mechanical properties as the remaining part. Figure 2 shows the calculation results in the upper part of the strip symmetrical along the x -axis of the thermal–mechanical coupling field temperature during the rolling process of the heated rolls. The inlet thickness is 16 mm, the roll surface temperature is 350 °C, the strip temperature is 20 °C, the rolling speed is 0.01 m/s, and the reduction is 20%. As can be seen from the figure, under stable rolling conditions, the temperature of the strip surface rises steadily in the rolling direction as the hot rolls come into contact with the strip. Under the heat conduction between the hot rolls and the strip surface, the temperature inside the strip rises gradually. As the heat conduction needs to take some time, the temperature of the strip surface in the front slip zone is higher than that of the strip core. As the rolling process proceeds, the temperature distribution of the section gradually tends to be uniform, and the temperature of the section at the outlet end of the strip can reach nearly 180 °C. If the plate thickness, speed, and other parameters of the HSR-HR process can be reasonably controlled, the temperature conditions of magnesium alloy recrystallization kinetics can be satisfied.

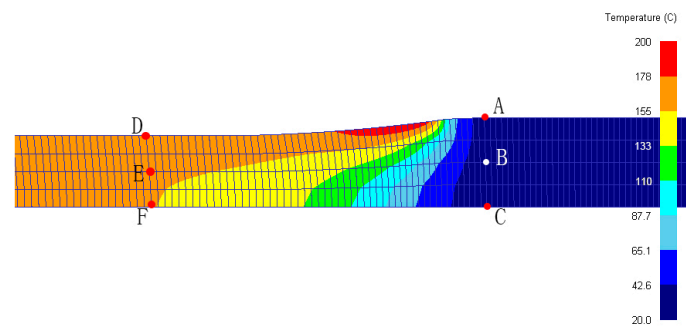


Figure 2. Temperature distribution of the upper strip symmetrically along the x-axis.

Figure 3a shows the temperature variation of the strip along the path AD, BE, CF, where AD, BE, and CF represent the rolling direction paths at the surface of the strip, at the 1/4 thickness of the strip, and the core of the strip, respectively, as shown by the connecting lines of AD, BE, CF in the strip in Figure 2. The strip typical points A, B, and C with the time of the temperature change curve are shown in Figure 3b in which when the strip rolling process enters the steady state, the temperature at the inlet end rises from the normal temperature to about 40 °C due to the contact heat exchange between the rolls and the strip, and the surface and core temperatures are the same. As shown in Figure 3a, the strip surface temperature change from the inlet end to the outlet end after strip biting first increases rapidly and then tends to stabilize. The temperature difference between the strip surface and the core is about 140 °C after the strip bite, which is due to the thicker workpiece and longer heat transfer time. Under the effect of heat conduction, the temperature of the core also increases significantly. Due to the effect of air cooling and heat conduction, when the deformed end is close to the outlet end, the temperature of the strip surface decreases slightly, while the temperature of the core rises as the temperature of the thickness part tends to stabilize. From Figure 3b, the temperature rise at the surface and in the core is divided into three essentially identical phases: a slow rise (Area I labeled in Figure 3b, a fast rise (Area II), and a thermal equilibrium phase (Area III).

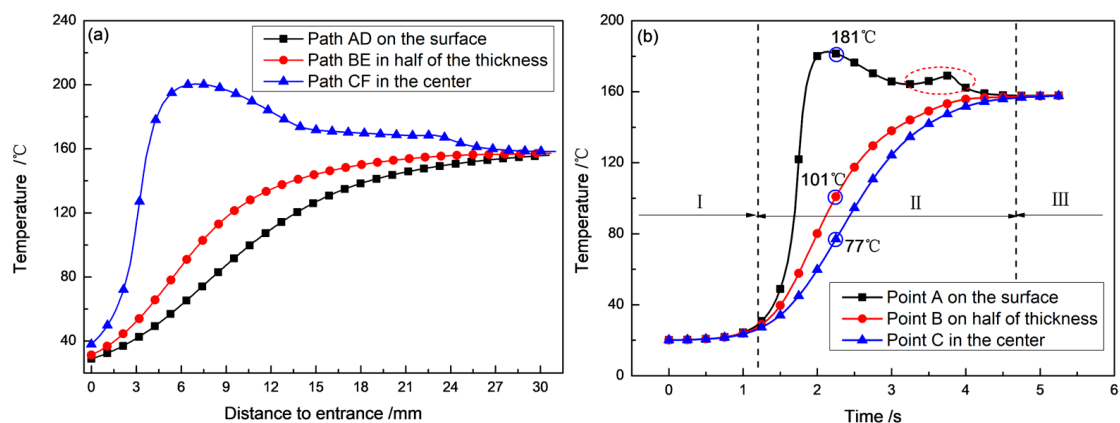


Figure 3. Temperature changes: (a) distribution along the path; (b) temperature–time curve of typical points.

In the first stage, under the action of heat conduction, the heated strip in the deformation zone transfers heat slowly to the point that does not enter the deformation zone. In the second stage, due to the direct heat transfer of metal particles from the roll surface into the deformation zone of the second stage, the temperature of the strip rises rapidly, the maximum speed of the strip surface heating exceeds 180 °C/s, and the maximum speed of the core heating is about 50 °C/s or more. Because of that, magnesium alloy has good thermal conductivity, which is helpful for the development of the heated-roll rolling process. After the strip surface temperature reaches the peak, it begins to decline, and

then begins to rise again near the center point under the effect of improving the contact heat exchange efficiency; as the rolling process continues, when the particle temperature of the deformation zone reaches a certain value, the heat input of the roll facing the strip surface and the heat conduction of the strip to the core part of the strip reaches a thermal equilibrium, and the temperature distribution of the strip tends to be stabilized until the end of the deformation.

3.2. Mechanical Analysis

Figure 4 shows the distribution of mechanical and deformation parameters in the rolling process of the heated roll. As can be seen from the figure, in the heated-roll rolling process, there is no obvious stress concentration in the effective stress (von Mises stress) distribution, the area with large stress is close to the interface of the rigid-plastic intersection at the entrance end, and the stress value is about 199 MPa. Under the condition of hot-roll rolling, due to the direct heat transfer from the roll to the rolled piece, the strip temperature increases rapidly, making the softening play a leading role, and the stress value gradually decreases from the middle of the deformation zone to the inlet and outlet end. The effective strain (von Mises strain) increases gradually from the inlet to the outlet end, the strain value of the strip surface is larger than that of the center at the front slip area, and the strain value of the strip surface is slightly smaller than that of the center at the back slip area. The effective strain rate increases first from the inlet end to the outlet end and then decreases. Different strain rates of each particle in the deformation zone lead to uneven deformation during rolling. Velocity singularity occurs easily in the region near the neutral point due to relative velocity discontinuity, where the deformation rate is small and the neutral point is near the outlet. The velocity field distribution law is close to the effective strain distribution law, and there is a certain discontinuity in the section velocity along the thickness direction in the region near the interface of the rigid-plastic intersection.

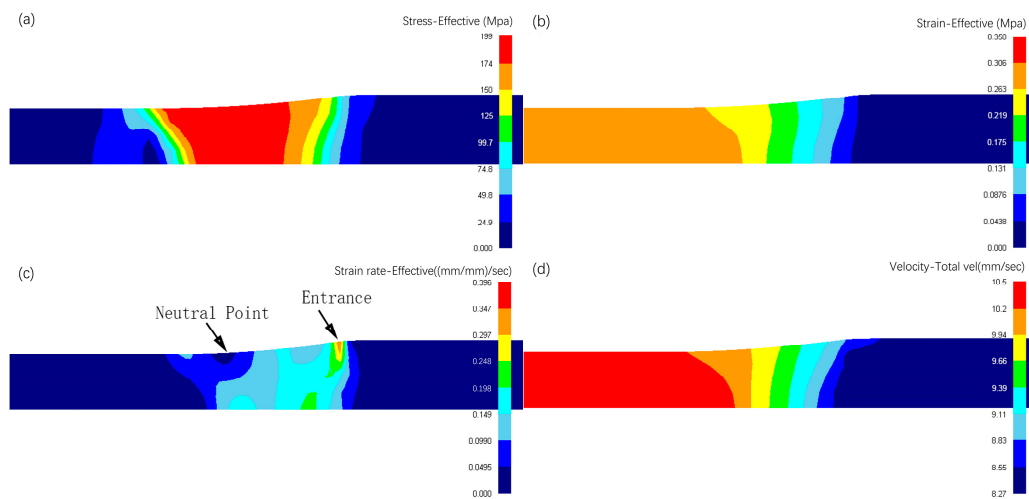


Figure 4. Distribution of deformation parameters: (a) effective stress; (b) effective strain; (c) effective rate of change; (d) speed.

The rolling process contact surface pressure distribution and rolling load changes are shown in Figure 5. As can be seen from the figure, the pressure on the contact surface is not evenly distributed from the inlet end to the outlet end. The sudden change in velocity causes a significant peak at the rigid-plastic interface and in the region near the neutral point (the peak point is shown as the blue dotted line in Figure 5a). As can be seen from the area indicated by the red arrow on the right side of Figure 5a, there is an obvious red area in the just-bitten-in plastic deformation zone, indicating that the deformation is larger here, the velocity mutation is serious, and the contact pressure on the contact surface is about 312 MPa at the maximum. The abrupt velocity change at the interface of the rigid-plastic intersection near the outlet and the neutral point is relatively weak, and the peak pressure at

the contact surface is about 260 MPa. According to Equation (4), the heat transfer coefficient is related to contact pressure, so hot rolls and rolling load changes are shown in Figure 5. The peak pressure is small, about 260 MPa; according to Equation (4), it can be seen that the heat transfer coefficient is related to the contact pressure, so there are three peaks of the heat transfer rate on the contact surface along the contact arc length in the hot-roll rolling process, proving once again that there is a peak heat transfer efficiency near the neutral point during the hot-roll rolling process. As can be seen from Figure 5b, the rolling process load change is roughly divided into three stages. In the first stage, the billets undergo plastic deformation and gradually fill the deformation zone during the strip biting, and the rolling load increases sharply, reaching a peak value of about 4470 N; in the second stage, the strip is warmed up under the action of the work rolls and enters the stable rolling stage, the softening and hardening of the strip are almost in dynamic equilibrium, and the rolling load is kept unchanged; in the third stage, the flow of metal in the deformation zone is reduced, and the load begins to fall gradually with the gradual end of the rolling process.

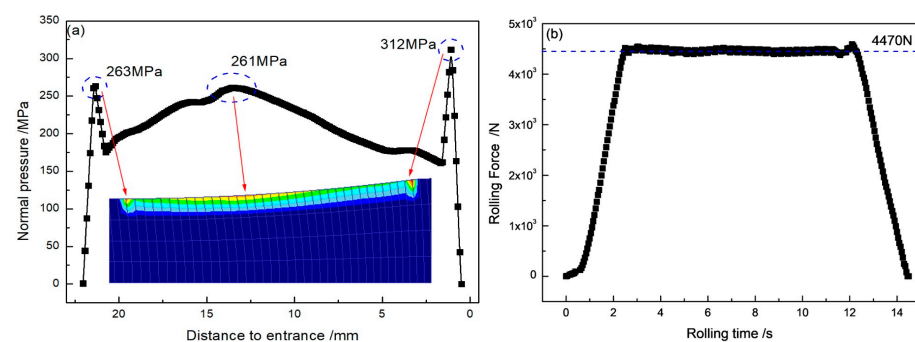


Figure 5. Contact pressure and load–time curve: (a) normal pressure; (b) modeling of rolling force.

3.3. Temperature

Temperature, strain, and deformation rate are the key factors affecting the plastic deformation behavior and microstructure evolution of magnesium alloy strips in the rolling process. Temperature, in particular, has a significant influence on the dynamic recrystallization process. The accurate prediction of the outlet temperature is of great significance for optimizing the rolling process parameters and obtaining magnesium alloy strips with good performance in the rolled state. Based on the results of numerical simulation, the effects of the rolling speed R_s , initial thickness of the strip I_t , undercutting rate R_r , and rolling surface temperature T_r on the temperature and strain rise of the hot rolled strip at room temperature are investigated. A mathematical model of the average temperature and equivalent change of the section nodes at the outlet end of rolling is established for the prediction of temperature and strain at the outlet end, where T_m is the average temperature of the section nodes at the outlet end and its expression is shown in Equation (5).

$$T_m = \frac{1}{n} \sum_{i=1}^n T_i \quad (5)$$

where T_m is the average temperature of the outlet end section node, °C; T_i is the temperature of the outlet end section node, °C; and n is the number of outlet section nodes.

The key to establishing the temperature prediction model is to find the functional relationship between the average temperature at the outlet end and different variables, which is described in Figure 6 by calculating the fitting curve between the temperature and the variables. According to Figure 6a, it can be seen that the temperature difference between the roll and the strip is larger as the temperature of the roll surface increases, and the heat transfer efficiency is higher. Additionally, from Figure 6b, it can be seen that as the reduction increases, the deformation contact area between the roll and the strip increases, and the distance from the surface to the center of the heat transfer decreases. Therefore, with the rise in the roll surface temperature and reduction, the average temperature at the

outlet end rises linearly, so the average temperature at the outlet end is linearly fitted to the roll surface temperature T_r and the depression rate R_r . As can be seen from Figure 6c,d, with the increase in rolling speed, the contact heat transfer time is insufficient, and the initial thickness increases the distance from the surface heat transfer to the center, resulting in an exponential decrease in the value of the average temperature at the outlet end with the increase in rolling speed R_s and initial thickness I_t . The strip outlet temperature is most sensitive to the rolling speed, followed by the initial thickness, according to the change in the slope of the relationship curve. The predictive model equation for the outlet end temperature that can be derived from the fitting curve between the average temperature at the outlet end and the influencing factors of different variables is shown in Equation (6). The fitting variance of the average temperature relationship curve is greater than 0.99, showing that the fitting accuracy is very good and the results are trustworthy.

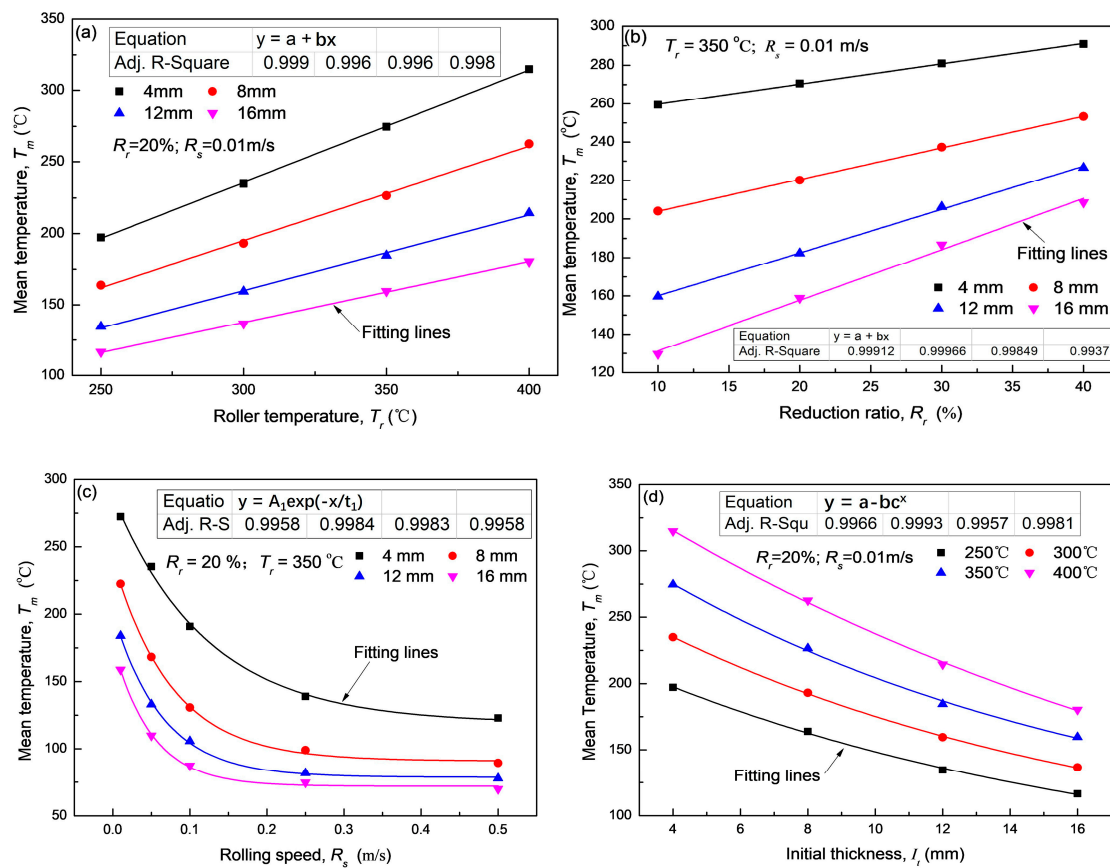


Figure 6. The influence of variable parameters on average temperature and fitting curve: (a) $T_m - T_r$; (b) $T_m - R_r$; (c) $T_m - R_s$; (d) $T_m - I_t$.

According to the relationship curve between the average temperature and the influencing factors of different variables, the average temperature T_m can be described as follows:

$$T_m = A_0(T_r)^{B_0}(R_r)^{C_0} \exp(D_0 \cdot R_s^{0.05} + E_0 \cdot I_t) \quad (6)$$

Here, T_m with T_r and R_r is a linear fitting relationship, so the formula is expressed as a linear relationship, and A_0 , B_0 , and C_0 are set as unknown constant values. T_m with I_t and R_s is an exponential fitting relationship, so the formula is expressed as an exponential relationship, and to accurately reflect the strong nonlinearity of the influence of rolling speed R_s changes on temperature, and to improve the accuracy of the linear fitting, the rolling speed was first power-squared and then linearly fitted. By analyzing the variance of the linear fitting results under different power cube indices, the better power cube index is set to 0.05. As shown in Figure 7c, when the power cube index of R_s is taken as 0.05, the

average fitting variance of the four curves is 0.9604. The coefficients of R_s and I_t are set to be the unknown constant values, and the temperature prediction model is obtained by finding the values of $A_0, B_0, C_0, D_0,$ and E_0 .

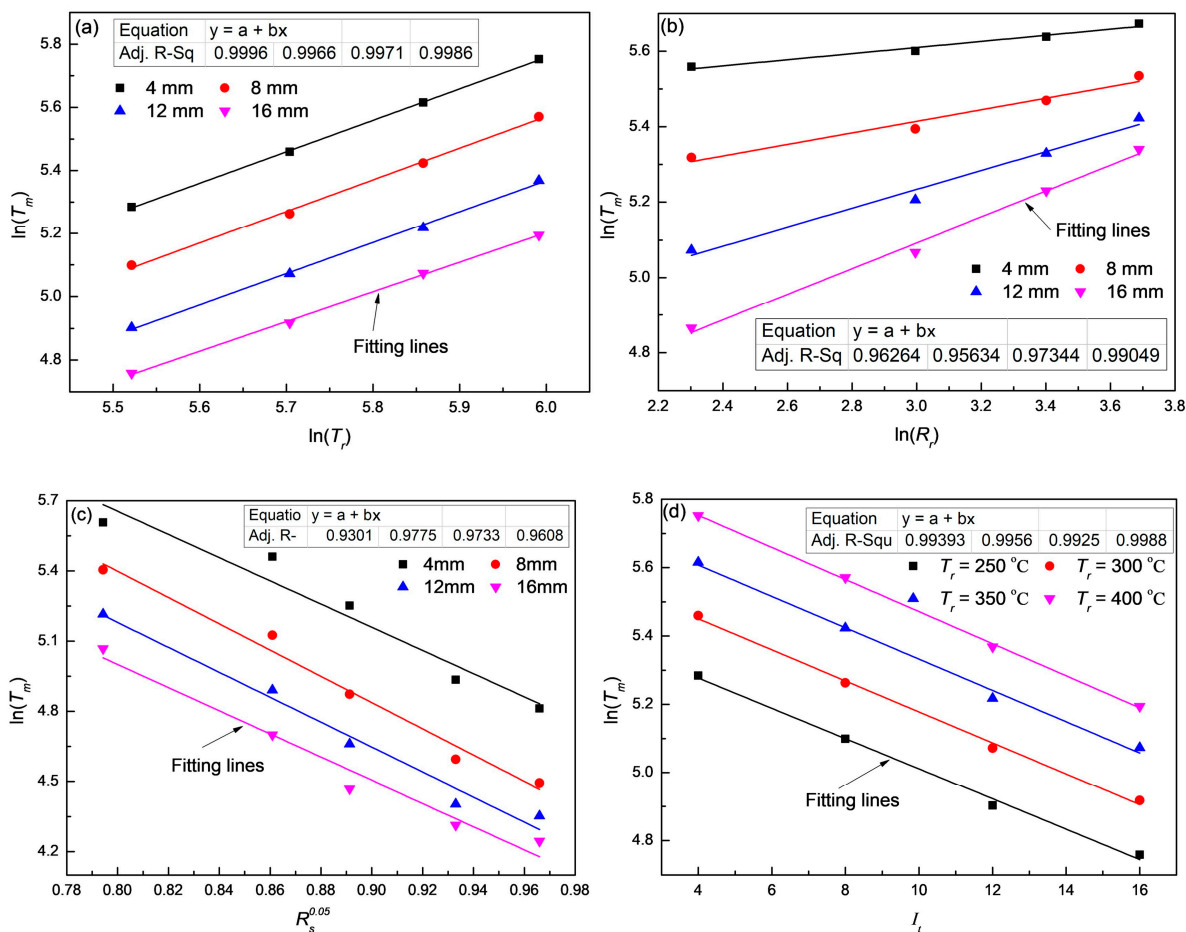


Figure 7. The relationship between different variables: (a) $\ln(T_m) - \ln(T_r)$, (b) $\ln(T_m) - \ln(R_r)$, (c) $\ln(T_m) - (R_s)^{0.05}$, (d) $\ln(T_m) - (I_t)$.

Therefore, a natural logarithm is taken at both ends of Equation (6) to obtain Equation (7).

$$\ln(T_m) = \ln(A_0) + B_0 \ln(T_r) + C_0 \ln(R_r) + D_0 (R_s^{0.05}) + E_0 (I_t) \tag{7}$$

According to Formula (7), the expressions for $B_0, C_0, D_0,$ and E_0 are $B_0 = \partial \ln(T_m) / \partial \ln(T_r)$, $C_0 = \partial \ln(T_m) / \partial \ln(R_r)$, $D_0 = \partial \ln(T_m) / \partial (R_s^{0.05})$, and $E_0 = \partial \ln(T_m) / \partial (I_t)$. Their values are, respectively, the linear fitting slopes of the relationship curves for $\ln(T_m) - \ln(T_r)$, $\ln(T_m) - \ln(R_r)$, $\ln(T_m) - (R_s)^{0.05}$, and $\ln(T_m) - I_t$ (Figure 7).

The average slope of linear fitting in Figure 7 shows that $B_0, C_0, D_0,$ and E_0 are 0.98, 0.207, $-0.228,$ and -0.046 , respectively. The lowest fitting variance is 0.93, indicating a high fitting accuracy and reliable results.

The parameter values of $B_0, C_0, D_0,$ and E_0 were calculated by Equation (7), and their values were inserted into Equation (6). It can be seen that A_0 is the linear fitting slope of T_m and the expression $\{(T_r)^{0.98} (R_r)^{0.207} \exp [-5.21 (R_s)^{0.05} - 0.046 I_t]\}$. Through linear fitting in Figure 8, it can be obtained that coefficient A_0 is 35.042 and the linear fitting variance is 0.97, showing that the fitting accuracy is reliable.

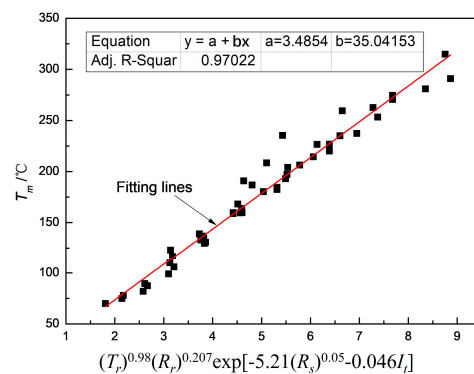


Figure 8. Relationship between T_m and $\{(T_r)^{0.98}(R_r)^{0.207} \exp[-5.21(R_s)^{0.05} - 0.046I_t]\}$.

After substituting the constant parameters into Equation (6), the functional equation for the average temperature T_m at the outlet end of the strip can be obtained:

$$T_m = 35.042 \cdot (T_r)^{0.98} \cdot (R_r)^{0.207} \cdot \exp[-5.21(R_s)^{0.05} - 0.046I_t] \quad (8)$$

Through correlation analysis and data comparison validation (Figure 9), it can be seen that there is a good agreement between the temperature data from the original experiments and the predicted values from the mathematical model built using finite element data.

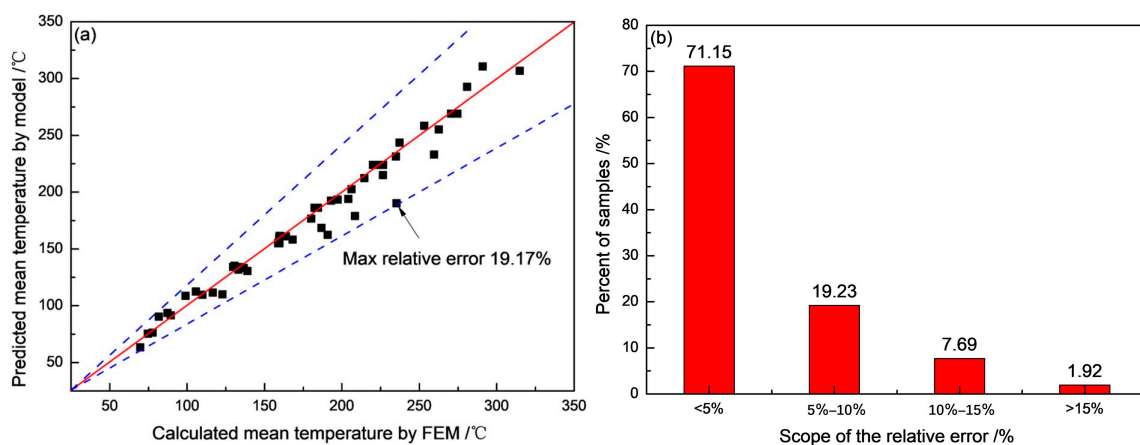


Figure 9. Relative error analysis of the prediction model. (a) Chart of consistency between original data and predicted values. (b) Percentage of different error ranges between original data and predicted values in the sample.

In Figure 9a, the solid red line is a ray with a slope of 1, indicating that the error between the original data and the predicted value is 0. The blue dotted line is a ray emanating from the origin towards the data furthest from the solid red line, which indicates the extent to which the data deviate from the error of 0. The two blue rays in the figure constitute the relative error range of the data. Therefore, from Figure 9a, it can be calculated that the maximum relative error was about 19.17% and the average relative error was about 4.17%. Figure 9b shows the proportion of the error range between the original data and the predicted value in the sample. As shown in Figure 9b, more than 90% of the total relative errors between the data and the predicted values were less than 10%. The prediction accuracy of the model is high, and the predictive model for the temperature at the outlet end based on linear fitting and nonlinear regression methods is trustworthy.

3.4. Experimental Validation and Application of the Model

To further confirm the validity of the developed model, experiments on the rolling process were carried out under various rolling conditions. Roll outlet temperatures were

measured with Raytek thermometers (3ILTDL3U). The infrared ray of the thermometer was aimed at the outlet end of the strip (as shown in Figure 10); then, three sets of data were measured when the rolling was stabilized, and the average value was taken.



Figure 10. Aiming point of the pyrometer at the strip outlet section.

A comparison of the measured temperatures at the outlet end and the model predictions under different rolling conditions is depicted in Figure 11. The data processing for Figure 11 was the same as that for Figure 9a, so the explanations above concerning Figure 9a can be referred to for the significance of the colored rays in Figure 11. Figure 11 shows that the model-predicted temperature values at the outlet end are in good agreement with the measured data, and for the predicted results, relative errors of less than 10% account for 90% of the total data.

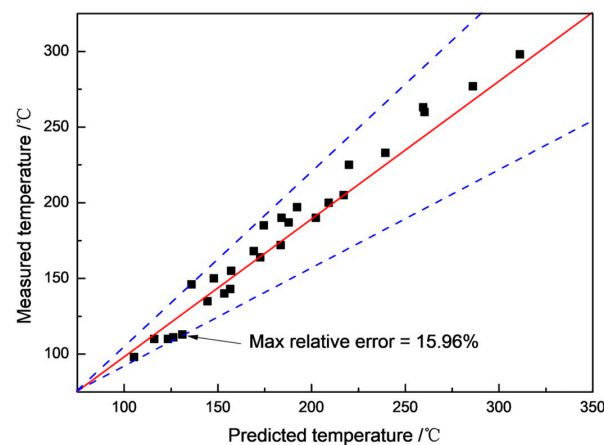


Figure 11. Comparison of predicted and measured temperatures.

The maximum relative error of the prediction results is about 15.96%, and the average relative error is about 6.1%. The constructed model can achieve an accurate prediction of the strip outlet end temperature, which in turn provides a reference for the regulation and optimization of the hot rolling process.

In addition, modeling techniques and methods are useful for the nonlinear analysis of engineering problems. For the variable values that are affected by some output parameters during the rolling process, the relationship equations between these parameters and variables can be modeled by the nonlinear regression and linear fitting methods proposed in this paper.

In addition, if the other parameters and the ideal mean temperature of the NSR-HR process are known, Figure 12 provides an additional important aid in calculating the critical values for any of the influencing parameters.

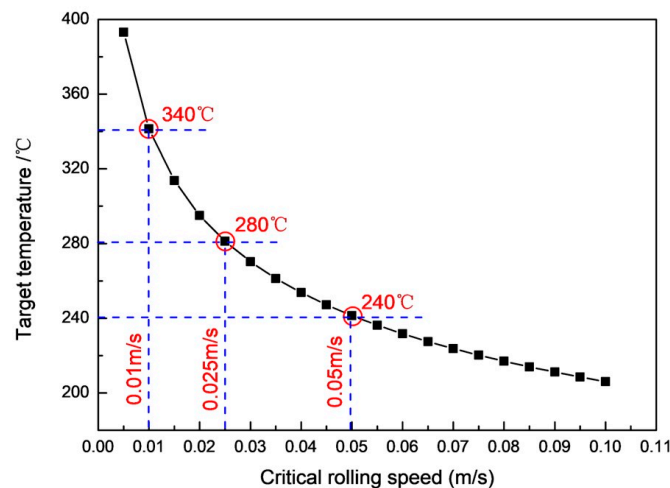


Figure 12. Relationship between target temperature and critical rolling speed.

For example, when the initial thickness is 6 mm, the reduction is set at 30%, the rolling temperature is 400 °C, and the ideal average temperatures are 240 °C, 280 °C, and 320 °C. Then, according to the prediction model, the critical rolling speeds should be approximately 0.05 m/s, 0.025 m/s, and 0.01 m/s (Figure 12).

4. Conclusions

- (1) When the metal particles transfer heat directly from the surface of the rolls, the temperature of the strip surface and core enters the rapid rise stage, at which time the maximum rate of temperature rise in the core is about 50 °C/s or more. When the strip approaches the outlet end, the surface temperature decreases slightly, but the core part continues to be heated until it reaches thermal equilibrium, and the cross-section temperature tends to be constant. Magnesium alloy has good thermal conductivity, and reasonable control of rolling parameters can realize dynamic recrystallization grain refinement of magnesium alloy strips through HSR-HR continuous large plastic deformation.
- (2) In the process of NSR-HR, the direct heat transfer from the roll to the rolled part makes the softening play a dominant role, and the stress value gradually decreases from the middle of the deformation zone to the inlet and outlet ends. The strain value of the strip surface is larger than that of the center at the front slip area, and the strain value of the strip surface is slightly smaller than that of the center at the back slip area. The constant velocity variation increases first and then decreases from the inlet end to the outlet end, and the strain rate of each particle in the deformation zone is different during the rolling process, resulting in uneven deformation.
- (3) The average temperature at the strip outlet rises linearly with the increase in rolling temperature and reduction. The average temperature at the strip outlet decreases exponentially with the increase in rolling speed and initial thickness. The outlet temperature is the most sensitive to the rolling speed, followed by the initial thickness. A prediction model of strip temperature for the hot rolling process including the rolling temperature, reduction rate, rolling speed, and initial thickness was constructed according to the variation rule of outlet temperature. The predicted temperature of the model is in good agreement with the experimental results, with relative errors of less than 10% accounting for 90% of the total data. The constructed temperature prediction model is reliable and capable of accurately predicting the strip outlet temperature during the hot rolling process. It can also realize the adjustment and optimization of hot rolling process parameters under known ideal temperature conditions. In addition, the fitting methods provide references of theoretical significance for modeling parametric equations and nonlinear relationships among variables in other plastic processing processes.

Author Contributions: R.M.: Data Analysis; L.C.: Manuscript Writing; L.B.: Data Collection, Chart Making; C.L.: Research Design; X.L.: Literature Retrieval. All authors have read and agreed to the published version of the manuscript.

Funding: This research was funded by the Natural Science Foundation, Steel and Iron Foundation of Hebei Province (E2018501016).

Data Availability Statement: The data that support the findings of this study are available on request from the corresponding author; please contact meirubin@neuq.edu.cn.

Conflicts of Interest: The authors declare that there are no conflict of interest.

References

1. Sakai, T.; Belyakov, A.; Kaibyshev, R.; Miura, H.; Jonas, J.J. Dynamic and post-dynamic recrystallization under hot, cold and severe plastic deformation conditions. *Prog. Mater. Sci.* **2014**, *60*, 130–207. [\[CrossRef\]](#)
2. Xu, T.; Yang, Y.; Peng, X.; Song, J.; Pan, F. Overview of advancement and development trend on magnesium alloy. *J. Magnes. Alloys* **2019**, *7*, 536–544. [\[CrossRef\]](#)
3. Singh, N.; Batra, U.; Kumar, K.; Ahuja, N.; Mahapatro, A. Progress in bioactive surface coatings on biodegradable Mg alloys: A critical review towards clinical translation. *Bioact. Mater.* **2023**, *19*, 717–757. [\[CrossRef\]](#)
4. Miyano, H.; Takemoto, K.; Tsushida, M.; Kitahara, H.; Ando, S. Evaluation of Non-Basal Slip Activity in Rolled Mg-Li Alloys. *Mater. Trans.* **2021**, *62*, 1097–1101. [\[CrossRef\]](#)
5. Han, S.; Li, Z.; Wang, Z.; Li, Y. Review on joining processes of magnesium alloy sheets. *Int. J. Adv. Manuf. Technol.* **2022**, *118*, 2787–2803. [\[CrossRef\]](#)
6. Pan, F.; Jiang, B. Development and Application of Plastic Processing Technologies of Magnesium Alloys. *Acta Metall. Sin.* **2021**, *57*, 1362–1379. [\[CrossRef\]](#)
7. Humphreys, F.J.; Prangnell, P.B.; Priestner, R. Fine-grained alloys by thermomechanical processing. *Curr. Opin. Solid State Mater. Sci.* **2001**, *5*, 15–21. [\[CrossRef\]](#)
8. Bi, X.; Hu, Y.; Li, R.; Zhao, H.; Li, T. A novel method for preparing Al/Mg/Al laminated composite material, processing maps and interface diffusion analysis. *J. Alloys Compd.* **2022**, *900*, 163417. [\[CrossRef\]](#)
9. Gao, H.-T.; Kong, C.; Yu, H.-L. Lightweight metal laminated plates produced via (hot, cold and cryogenic) roll bonding: A review. *Trans. Nonferrous Met. Soc. China* **2023**, *33*, 337–356. [\[CrossRef\]](#)
10. Pan, F.; Zeng, B.; Jiang, B.; Zhang, M.; Dong, H. Enhanced mechanical properties of AZ31B magnesium alloy thin sheets processed by on-line heating rolling. *J. Alloys Compd.* **2017**, *693*, 414–420. [\[CrossRef\]](#)
11. Chen, W.Z.; Zhang, W.C.; Zhang, L.X.; Wang, E.D. Property improvements in fine-grained Mg-Zn-Zr alloy sheets produced by temperature-step-down multi-pass rolling. *J. Alloys Compd.* **2015**, *646*, 195–203. [\[CrossRef\]](#)
12. Guo, J.; Sun, W.; Xiang, N.; Chen, F. Interfacial Bonding and Fracture Behaviors of AZ63 Magnesium Alloy Sheet Processed by Accumulative Roll Bonding. *Materials* **2023**, *16*, 4981. [\[CrossRef\]](#)
13. Li, Z.; Jiang, H.; Wang, M.; Jia, H.; Han, H.; Ma, P. Microstructure and Mechanical Properties of Al-Mg-Si Similar Alloy Laminates Produced by Accumulative Roll Bonding. *Materials* **2021**, *14*, 4200. [\[CrossRef\]](#)
14. Mehr, V.Y.; Toroghinejad, M.R. On the texture evolution of aluminum-based composites manufactured by ARB process: A review. *J. Mater. Res. Technol.-JmrT* **2022**, *21*, 1095–1109. [\[CrossRef\]](#)
15. Lee, S.-E.; Kim, M.-S.; Chae, Y.-W.; Guim, H.; Singh, J.; Choi, S.-H. Effect of intermediate heat treatment during hot rolling on the texture and formability of annealed AZ31 Mg alloy sheets. *J. Alloys Compd.* **2022**, *897*, 163238. [\[CrossRef\]](#)
16. Wang, R.; Xu, Z.; Jiang, Y.; Tang, G.; Wan, J.; Li, Q. Design high-performance AZ31 ultrathin strip through multi-pass electroplastic rolling without off-line annealing. *Mater. Sci. Eng. A-Struct. Mater. Prop. Microstruct. Process.* **2023**, *862*, 144510. [\[CrossRef\]](#)
17. Fisher, R.B. A rolling mill with heated roll device. *Heavy Mach.* **1964**, *13*, 30–32. [\[CrossRef\]](#)
18. Mei, R.-B.; Bao, L.; Huang, F.; Zhang, X.; Qi, X.-W.; Liu, X.-H. Simulation of the flow behavior of AZ91 magnesium alloys at high deformation temperatures using a piecewise function of constitutive equations. *Mech. Mater.* **2018**, *125*, 110–120. [\[CrossRef\]](#)
19. Fukuoka, H.; Huang, X.; Suzuki, K.; Tsukada, Y.; Koyama, T.; Chino, Y. Effect of Rolling Temperature on Room Temperature Formability and Texture Formation of Mg-3 mass%Al-1 mass%Sn Alloy Sheet. *J. Jpn. Inst. Met. Mater.* **2021**, *85*, 120–127. [\[CrossRef\]](#)
20. Li, R.; Xiao, Z.; Li, Z.; Meng, X.; Wang, X. Work Hardening Behavior and Microstructure Evolution of a Cu-Ti-Cr-Mg Alloy during Room Temperature and Cryogenic Rolling. *Materials* **2023**, *16*, 424. [\[CrossRef\]](#)
21. Vignesh, P.; Abraham, A.; Kumaran, S. Microstructural correlation of cross rolling temperature of AT55 magnesium alloy in mechanical and formability behaviour. *Micron* **2022**, *160*, 103305. [\[CrossRef\]](#)
22. Wang, J.; Guo, L.; Wang, C.; Zhao, Y.; Qi, W.; Yun, X. Prediction of Dynamically Recrystallized Microstructure of AZ31 Magnesium Alloys in Hot Rolling Using an Expanded Dislocation Density Model. *J. Mater. Eng. Perform.* **2023**, *32*, 2607–2615. [\[CrossRef\]](#)
23. Yu, C.; He, Z.; Lv, Q.; Yu, J.; Xiao, H. Preparation of Ti/Al composite plates by differential temperature rolling with induction heating. *Int. J. Adv. Manuf. Technol.* **2021**, *117*, 383–394. [\[CrossRef\]](#)

24. Zhou, L.; Wu, Z.; Li, Y.; Yao, H.; Liu, Y.; Yuan, Y.; Meng, W.; Han, L.; Cao, X. Temperature characteristics of indentation rolling resistance of belt conveyor. *J. Mech. Sci. Technol.* **2023**, *37*, 4125–4135. [[CrossRef](#)]
25. Cai, L.; Feng, Y.; Lu, Y.-T.; Lin, Y.-F.; Hung, T.-P.; Hsu, F.-C.; Liang, S.Y. Analytical Model for Temperature Prediction in Milling AISI D2 with Minimum Quantity Lubrication. *Metals* **2022**, *12*, 697. [[CrossRef](#)]
26. Yu, H.-L.; Yu, Q.-B.; Kang, J.-W.; Liu, X.-H. Investigation on Temperature Change of Cold Magnesium Alloy Strips Rolling Process with Heated Roll. *J. Mater. Eng. Perform.* **2012**, *21*, 1841–1848. [[CrossRef](#)]
27. Sun, T.; Li, J.-P. Method for Outlet Temperature Control during Warm Rolling of AZ31 Sheets with Heated Rolls. *Isij Int.* **2017**, *57*, 1577–1585. [[CrossRef](#)]
28. Zou, J.-F.; Ma, L.-F.; Zhang, G.-H.; Huang, Z.-Q.; Lin, J.-B.; Liu, P.-T. Controlling Roll Temperature by Fluid-Solid Coupled Heat Transfer. *Chin. J. Mech. Eng.* **2018**, *31*, 93. [[CrossRef](#)]
29. Lee, H.-W.; Yoo, J.-H.; Kwon, Y.-C.; Kang, J.-H. Calculation Method for Cold Flow Stress of Al6082 Based on Tensile Test and Compression Test Results. *Int. J. Precis. Eng. Manuf.* **2021**, *22*, 1337–1344. [[CrossRef](#)]
30. Romanova, T.P.; Yankovskii, A.P. Structural model for spatially and flatly reinforced medium of rigid-plastic materials considering three-dimensional stress state in all components. *Mech. Adv. Mater. Struct.* **2022**, *29*, 2668–2679. [[CrossRef](#)]
31. Yu, Z.; Zhu, C.; Chen, M.; Luo, S.; Ma, C. 3D FE modeling simulation of the double-roll hot rotary forging of large diameter thin-walled metal disk. *Int. J. Adv. Manuf. Technol.* **2022**, *123*, 2123–2137. [[CrossRef](#)]
32. Ding, Y.; Zhu, Q.; Le, Q.; Zhang, Z.; Bao, L.; Cui, J. Analysis of temperature distribution in the hot plate rolling of Mg alloy by experiment and finite element method. *J. Mater. Process. Technol.* **2015**, *225*, 286–294. [[CrossRef](#)]
33. Raghunath, B.K.; Raghukandan, K.; Karthikeyan, R.; Palanikumar, K.; Pillai, U.T.S.; Gandhi, R.A. Flow stress modeling of AZ91 magnesium alloys at elevated temperature. *J. Alloys Compd.* **2011**, *509*, 4992–4998. [[CrossRef](#)]

Disclaimer/Publisher’s Note: The statements, opinions and data contained in all publications are solely those of the individual author(s) and contributor(s) and not of MDPI and/or the editor(s). MDPI and/or the editor(s) disclaim responsibility for any injury to people or property resulting from any ideas, methods, instructions or products referred to in the content.